Comparing Well and Geophysical Data for Temperature Monitoring within a Bayesian Experimental Design Framework

Robin Thibaut[1], Nicolas Compaire[2], Nolwenn Lesparre[3], Maximilian Ramgraber[4], Eric Laloy[5], Thomas Hermans[1]

[1]Ghent University, Belgium
[2]Institut des Sciences de la Terre, Université Grenoble Alpes, France
[3]Institut Terre et Environnement de Strasbourg, Université de Strasbourg, France
[4]Massachusetts Institute of Technology, USA
[5]SCK CEN, Belgium

Key Points:

- We propose a method for optimizing the design of a 4D temperature field monitoring experiment.
- We use Bayesian Evidential Learning (BEL) to infer the posterior distribution of the temperature field for the experiment design.
- We demonstrate how BEL can combine temperature logs and ERT data to assist in the design of experiments for a 4D temperature monitoring.

Corresponding author: Robin Thibaut, robin.thibaut@ugent.be

Abstract

Temperature logs are an important tool in the geothermal industry. Temperature measurements from boreholes are used for exploration, system design, and monitoring. The number of observations, however, is not always sufficient to fully determine the temperature field or explore the entire parameter space of interest. Drilling in the best locations is still difficult and expensive. It is therefore critical to optimize the number and location of boreholes. Due to its higher spatial resolution and lower cost, four-dimensional (4D) temperature field monitoring via time-lapse Electrical Resistivity Tomography (ERT) has been investigated as a potential alternative. We use Bayesian Evidential Learning (BEL), a Monte Carlo-based training approach, to optimize the design of a 4D temperature field monitoring experiment. We demonstrate how BEL can take into account various data source combinations (temperature logs combined with geophysical data) in the experimental design (ED). To optimize the ED and determine the best data source combination, we use the Root Mean Squared Error (RMSE) of the predicted target in the low dimensional latent space where BEL is solving the prediction problem. The generated models agree well with the true models and are accurate enough to be used in optimal ED. Furthermore, the method is not limited to monitoring temperature fields and can be applied to other similar experimental problems. The method is computationally efficient and requires little training data. A training set of only 200 is sufficient for the considered optimal design problem.

1 Introduction

Geothermal systems, including borehole thermal energy storage (BTES) and shallow aquifer thermal energy storage systems (ATES) are becoming more popular as the world looks for ways to reduce greenhouse gas emissions. Such systems use thermal energy extracted from the ground or groundwater to heat or cool buildings, which necessitates some electrical energy input for the heat pump, while storing the excess heat or cold underground. The goal is to re-use this thermal energy during the next season in a cyclic utilization (Saner et al., 2010; Vanhoudt et al., 2011; Bayer et al., 2013; Duijff et al., 2021). The performance of BTES and ATES strongly depends on the subsurface properties. Many variables are involved in geothermal processes, including porosity, hydraulic conductivity, thermal conductivity, and heat capacity. Subsurface temperature fluctuations are strongly influenced by the spatial distribution of these parameters, the boundary conditions, and the aquifer's hydraulic gradient when modeling the underground response under thermal stress (Ferguson, 2007; Bridger & Allen, 2010; W. Sommer et al., 2013; W. T. Sommer et al., 2014). Previous research demonstrated that time-lapse Electrical Resistivity Tomography (ERT) could monitor spatial temperature changes in the subsurface with a relatively large spatial coverage by utilizing variations in resistivity caused by temperature changes (Hermans et al., 2012, 2014; Arato et al., 2015; Hermans et al., 2015; Lesparre et al., 2019; Robert et al., 2019). In turn, ERT monitoring experiments can be used to predict the response of the subsurface to thermal exploitation (Hermans et al., 2018, 2019).

This paper presents a methodology for improving the design of field experiments using well and geophysical data by utilizing Bayesian Evidential Learning (BEL). BEL is a technique that combines Monte Carlo simulations and machine learning that can be used to improve the estimation of predictions uncertainty (Hermans et al., 2016, 2018; Michel et al., 2020; Thibaut et al., 2021). It solves the Bayesian inference in a low dimensional space using a relationship between predictor (data) and target (prediction) learned from a training set sampled from the prior distribution. Previous research has shown that BEL can estimate the posterior distribution of predictions in a variety of contexts, including geothermal systems (Hermans et al., 2018, 2019; Athens & Caers, 2019), contaminant transport (Satija & Caers, 2015; Scheidt et al., 2015), geophysical inversion Hermans et al. (2016); Michel et al. (2020). In addition, the BEL framework has

been successfully applied to a range of subsurface field cases, such as groundwater, shallow and deep geothermal and oil/gas predictions (J. Park & Caers, 2020; Pradhan & Mukerji, 2020; Tadjer & Bratvold, 2021). Its efficiency has been demonstrated with extensive synthetic validation, but also against rejection sampling (Scheidt et al., 2015), McMC algorithms (Michel et al., 2020, 2022), field data (Hermans et al., 2019), and experimental design (ED) (Thibaut et al., 2021).

Experimental design is the process of doing research in an objective and controlled manner in order to maximize precision.

There are many ways to solve ED problems, but the most classic method is by maximizing or minimizing a data utility function (e.g., Kikuchi et al. (2015)). However, the computational burden for this method is significant because ED requires solving the inverse problem for any possible outcome of the unknown data (e.g., Leube et al. (2012); Neuman et al. (2012)). To make practical applications tractable, two main simplifications have been proposed: (1) Bayesian Model Averaging (BMA) combined with preposterior estimation (Raftery et al., 2005; Vrugt & Robinson, 2007; Tsai & Li, 2008; Wöhling & Vrugt, 2008; Neuman et al., 2012; Kikuchi et al., 2015; Pham & Tsai, 2016; Samadi et al., 2020), and (2) surrogate modelling (Razavi et al., 2012; Laloy et al., 2013; Asher et al., 2015; Babaei et al., 2015; Zhang et al., 2015; Tarakanov & Elsheikh, 2020; Zhang et al., 2020).

It is commonly understood that stochastic approaches should be utilized to evaluate the complete range of potential outcomes, allowing a comprehensive risk assessment to serve as the basis for decision-making (de Barros et al., 2012; Zhou et al., 2014; Linde et al., 2017). A limitation of these approaches is the high computational burden associated with stochastic methods. Regardless, iterative approaches requiring multiple forward problem runs, such as Markov chain Monte Carlo (McMC) methods, are commonly used to solve the problem (Laloy & Vrugt, 2012; Vrugt, 2016).

BEL can be used to optimize the design of experiments for any cost function. In other words, it can be used to identify the most informative data set at a low computational cost (Thibaut et al., 2021). Within this context, BEL's main advantage is that the inferred relationship can be applied to any data set that is aligned with the prior distribution. It is useful in ED because the prediction problem can be solved readily, without any costly computation, for any new proposed data set. Thibaut et al. (2021) showed how BEL can be used to predict the wellhead protection area (WHPA) around pumping wells. A small number of tracing experiments (predictors) and the hydraulic conductivity (K) distribution were used to predict the WHPA. The Modified Hausdorff Distance (MHD) and Structural Similarity (SSIM) index metrics were used as data utility function to optimize the ED and find the optimal combination of data sources.

In this contribution, we propose a methodology for solving an optimal design problem involving two different data types, using the BEL framework. This study is based on the monitoring of a heat injection-storage-pumping experiment monitored by time-lapse Electrical Resistivity Tomography (ERT) and well data mimicking the field experiment of Lesparre et al. (2019). The ED aims to determine which factors (such as the number and location of monitoring wells) have the greatest influence on the prediction of the temperature field, and to answer the question, "How many wells are needed to replicate the prediction accuracy of the geophysical data alone?" Although monetary costs are not included in this contribution, there is a tradeoff between non-invasive data acquisition methods such as ERT and invasive data acquisition methods such as drilling, with the latter being generally more expensive. Different data types do not have the same value. It is critical to determine whether drilling is required or if a simple geophysical survey will suffice, depending on the specific problem at hand. It can also be useful to know whether it is worthwhile to conduct a long geophysical survey and mobilize a large amount of equipment if we can use an existing borehole in the area.

This contribution is unique in four ways when compared to previous applications of BEL to ED:

1. We use two different type of predictors, geophysical and borehole data, which vary in time, to predict a four-dimensional target, the temperature field magnitude in the aquifer over time. It will first be demonstrated how to predict the target using each data set separately, and then
2. how to use them jointly. Because the predictors are of different types, the dimensionality reduction step in the pre-processing section is applied to each instance separately, and then concatenated before being fed to the learning algorithm. Furthermore,
3. the Transport Map method is used to sample in the low dimensional space.
4. The data utility function is calculated in the low dimensional latent space, without the need to back transform the data to its original space.

Overall, BEL is well-suited to solve the considered ED problem at a low cost (considering both time and computational demand).

2 Methodology

2.1 BEL

The BEL framework has been extensively explained in contributions such as Hermans et al. (2018) or Scheidt et al. (2018), and we will only summarize the fundamental principles in this contribution. The objective of BEL is to determine the target H's posterior probability distribution $p(H|D_{obs})$, conditioned on an observed predictor D_{obs}. Both the target and the predictor are real, multidimensional random variables. First, training sets of H and D are generated by sampling the prior distribution through forward modeling. Then, the target and the predictor are separately subjected to dimensionality reduction through Principal Component Analysis (PCA) and projected to the new principal component (PC) space. Next, Canonical Correlation Analysis (CCA) analyses the PCs to find their underlying correlations while transforming them to new, maximally correlated canonical variates (CVs). Given that the CVs' relationships describe the behavior of each target dimension for each predictor dimension, an observed data point can be used to infer the posterior distribution of each unknown target dimension. To do this, we first project the observation onto the data CV axes using the same transformations we derived for the data samples. Then, we implement separate conditioning operations for each bivariate distribution. This allows us to take into account the different relationships between the predictor and target dimensions, and ultimately infer the posterior distribution of the unknown target dimensions. Thibaut et al. (2021), for example, demonstrated how this can be easily accomplished using multivariate Gaussian inference, provided that the CVs' bivariate distributions are both Gaussian and linear. Kernel Density Estimation (KDE) is another method for approximating the bivariate distribution for each CCA dimension without requiring such assumptions to be verified (e.g., Hermans et al. (2019); Michel et al. (2020)). KDE, on the other hand, has two parameters that must be adjusted: the kernel type, which defines the shape of the distribution at each coordinate, and the kernel bandwidth, which describes the size of the kernel at each position. Transport maps (Spantini et al., 2017) form another method that allows to calculate the posterior distribution and is used in this work (§2.3.3).

2.2 Experimental setup

We present a method for estimating the posterior distribution of an unknown four-dimensional temperature field during a heat injection-storage-pumping experiment. The experiment has been described in Lesparre et al. (2019). In short, hot water was injected

at 3 m^3/h into an aquifer at a temperature of 42 °C for six hours, followed by another injection at 14.5 °C for 20 minutes. Then, it was stored in the aquifer for 92 hours, and then pumped back out for 16 hours and 15 minutes at a flow rate of 3 m^3/h. The goal was to track the evolution of temperature distribution in the aquifer over time. The experiment was monitored using time-lapse ERT and temperature data in wells. The time-varying predictor (measured voltage for ERT, direct temperature for wells) and the target (temperature distribution in the aquifer) are high-dimensional, and their relationship is non-linear. The synthetic study design is based on a real time-lapse ERT investigation during an injection-storage-pumping test at Hermalle-sur-Argenteau near Liège, Belgium. This study site is on the Meuse River's alluvial plain and has been extensively documented (Dassargues, 1997; Derouane & Dassargues, 1998; Brouyère, 2001; Hermans et al., 2015; Klepikova et al., 2016). By performing geothermal field experiments such as injection and hot water pumping tests, we can gain a better understanding of the aquifer's behavior Palmer et al. (1992); Macfarlane et al. (2002); Vandenbohede et al. (2009, 2011); Wagner et al. (2014); Wildemeersch et al. (2014); B.-H. Park et al. (2015); Klepikova et al. (2016). Combined with these tests, geophysical and thermal monitoring can track heat transfer in the aquifer. The location of injection wells is the focal point of the hydrogeological models used in this study. These models' grids are 60 meters in length in the known direction of natural aquifer flow and 40 meters in length in the perpendicular direction to that direction (Figure 1). The grid layers begin at the surface of the aquifer's saturated zone at a depth of 3 meters and conclude at the surface of the impermeable sole at 10 meters, respectively. Along the Z axis (depth), the space step is 0.5 meters. According to the X axis, the space step varies between 2.5 centimeters at the injection locations and 2.5 meters around the edges, with a finer refinement of 0.25 centimeters in a 3 meters radius around the injection points (hydraulic flow direction) and Y (perpendicular direction).

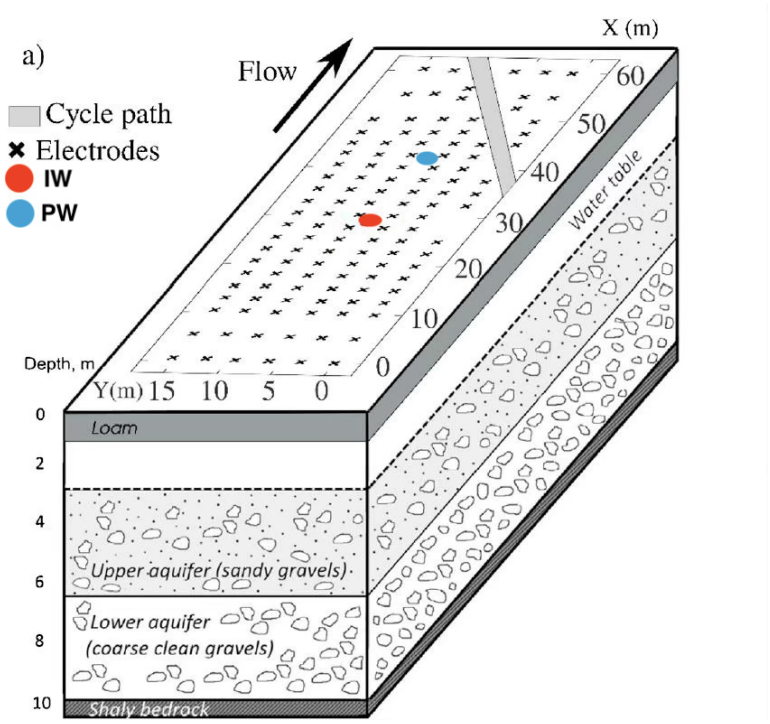

Figure 1. Model design (modified from Lesparre et al. (2019)) . IW = Injecting well. PW = Pumping well.

The average and variance of hydraulic conductivity (K), the anisotropy factor, and its direction in the horizontal plane and the range of the spherical variogram are used to build the models of the hydraulic conductivity distribution in the aquifer. In addition, the homogeneous porosity and the natural gradient are set as uncertain parameters. All other parameters including water and matrix thermal properties are set as constant. Bulk thermal properties are calculated based on porosity using the arithmetic average. The prior is the sum of all the definitions of the parameters under consideration. We detail the ranges of the variables in Table 1.

Uncertain parameter	**Range**
Log K mean	U[-1, -4], K in m/s
σ Log K	U[0.05,2], K in m/s
Effective porosity	U[0.05, 0.3]
Variogram main range	U[1, 10] m
Anisotropy ratio	U[0,0.5]
Orientation	U[0, π]
Natural gradient	U[0.0005, 0.00167]

Table 1. Parameters of the prior model

Each parameter is generated randomly and independently according to a uniform distribution. The sequential Gaussian simulation algorithm (Goovaerts, 1997) is then used to generate the hydraulic conductivity fields. In the direction of Y, the hydraulic flow at the grid boundaries is zero. It respects the natural gradient in the X-direction. For this investigation, 250 hydrogeological models were built and used to generate the temperature fields resulting from the injection-storage-pumping experiment. The HydroGeoSphere code was used to simulate the temperature field in the hydraulic conductivity grids during the injection-storage-pumping experiment (Brunner & Simmons, 2012). There are 106-time observations in each simulation. The temperature grids obtained are reduced to sub-grids around the injection well of size 16×16×14 of elementary volumes 0.5 m×0.5 m×0.5 m to reduce the amount of data. The temperature is averaged when the subgrid elemental volumes contain several elemental volumes from the initial grid. The temperature field is then transformed into a resistivity field using the inverted resistivity distribution from Lesparre et al. (2019) as a background and a change of resistivity with time uniquely dependent on the temperature variations produced by the model, following the approach described in Hermans et al. (2015). Then, the corresponding 250 simulations of the resistance variations corresponding to the ERT monitoring were computed with the EIDORS code (Polydorides & Lionheart, 2002). These simulations are generated by solving the direct problem with the following experimental setup: 6 parallel profiles of 21 electrodes in the X direction (natural flow direction in the aquifer), with a 2.5 meter spacing between the 17 central electrodes and a 5-meter spacing between the four electrodes at the profile's edge. For a total of 1948 quadrupoles, two types of geometry were used: multiple gradient geometry and dipole-dipole geometry. For each of the 106 temperature simulation time observations, an ERT simulation is generated for each model. The prediction for each model is thus made of 16×16×14 temperature grids for the 106 observation times, and the data is made of apparent resistivities measured by 1948 quadrupoles for the 106 observation times.

2.3 Heat prediction

2.3.1 Pre-processing

2.3.1.1 Target The target H is a three-dimensional temperature field subdivided into $\mathrm{n}_{rows} \times \mathrm{n}_{cols} \times \mathrm{n}_{lay}$ over n_{step} observation time steps. It is critical to reduce dimensionality because some small-scale variations of the target do not need to be perfectly reconstructed as they are already beyond the predictor's resolution. Before performing dimension reduction, the raw target is scaled to unit variance, because the dimension reduction step is sensitive to the scale of the data. The dimension reduction itself is done by linear PCA. The principal components are new variables produced by combining the initial variables in a linear way.

2.3.1.2 Predictor The geophysical predictor D_g is made up of resistance values measured by n_{quad} quadrupoles over n_{step} observation time steps, and the borehole predictor D_b is made of temperature curves measured at observation well's locations. Before performing dimension reduction, both raw predictors are scaled to unit variance. The dimension reduction is performed by linear PCA, and the number of components to keep is automatically set by setting the amount of variance that needs to be explained to 99%. The amount of variance is determined by the curve of the explained variance. When the explained variance reaches a plateau, the number of components is set to the number that corresponds to the explained variance at that point (not shown). When working with geophysical data, filtering higher dimensions allows to reduce the effect of noise on the prediction (Hermans et al. (2016); Michel et al. (2020)).

After dimensionality reduction, the PCs of both predictor and target are scaled to unit variance, because covariance matrices are sensitive to the scale of the data.

2.3.2 Training

After dimensionality reduction, the next step is to find the relationship between the predictor and the target in the reduced space. The CCA algorithm projects the data onto a new set of axes which maximize the correlation between the two data sets. The transformed variables are called Canonical Variates (CVs). Similarly to PCA, each pair of transformed variables is orthogonal (uncorrelated) with the other pairs. The CVs are the transformed variables representing the mutual information between the two data sets. Let δ be the number of PCs necessary to explain the required amount of variance in the predictor, and $\mathrm{n}_{training}$ be the number of pairs of predictors and targets used for training. In our case, δ is the sum of the number of components of the geophysical data and the borehole temperature curves, i.e., $\delta = \delta_g + \delta_b$. This is simply done by concatenating the geophysical and borehole temperature PCs into a single matrix. Following preprocessing, the model is trained with the CCA algorithm to establish a multivariate relationship between D and H in PC space. The number of CCA components η is set to δ, the maximum number that can be used (Meloun & Militký, 2012). The number of components to keep depends on the dimensionality reduction of the predictor. To allow back-transformation, more components must be used for the predictor than for the target before learning the relationship between the two. However, to avoid overfitting and noise propagation, it is recommended that both have a similar number of components. It does not have to be strictly the same. Let the superscript c denote the canonical space. The canonical variates (CVs) pairs are stored in the $(n_{training} \times \eta)$ matrices

$$D_\eta^c = d_{i,1}^c, d_{i,2}^c, \ldots, d_{i,\eta}^c | i = 1, \ldots, n_{training} \tag{1}$$

$$H_\eta^c = h_{i,1}^c, h_{i,2}^c, \ldots, h_{i,\eta}^c | i = 1, \ldots, n_{training} \tag{2}$$

With the pairs of canonical variates $\left(d_{:,1}^c, h_{:,1}^c\right) \sim \pi_1$ to $\left(d_{:,\eta}^c, h_{:,\eta}^c\right) \sim \pi_\eta$ established, we may infer the posterior in the canonical subspaces by independently condi-

tioning each of the resulting bivariate joint distributions $\pi_j, j = 1, \ldots, \eta$ on a new observation projected into the canonical predictor space $d^c_{new,j}$. In this study, we consider a new approach based on triangular transport, which offers a good tradeoff between computational efficiency and accuracy.

2.3.3 Conditioning with transport methods

In essence, transport methods seek a monotone, invertible transport map $\mathbf{S}$ that transforms samples from a target distribution π_j into samples from a simpler, user-specified reference distribution η, typically a standard multivariate normal distribution $N(0, I)$. This map allows us to sample conditionals of the target distribution, and thus implements the conditioning operation we are principally interested in. Transport methods are a nuanced topic, and the interested reader is referred to (Villani, 2009; El Moselhy & Marzouk, 2012; Spantini et al., 2017) for a more detailed discussion of their theoretical properties. In this study, we focus only on the parts necessary for the conditioning operation.

The map $\mathbf{S}$ is triangular, that is to say it consists of as many map components as there are dimensions in π_j (here: two, so $\mathbf{S} : \mathbb{R}^2 \to \mathbb{R}^2$), where each component depends on one more dimension than its predecessor. In our setting, the map is structured as:

$$\mathbf{S}\left(d^c_{:,j}, h^c_{:,j}\right) = \begin{bmatrix} S_1\left(d^c_{:,j}\right) \\ S_2\left(d^c_{:,j}, h^c_{:,j}\right) \end{bmatrix} = \begin{bmatrix} z_1 \\ z_2 \end{bmatrix} = \mathbf{z} \tag{3}$$

where $\mathbf{z}$ are samples distributed according to the reference η. If we are only interested in conditioning, we only need to define and optimize the second map component $S_2 : \mathbb{R}^2 \to \mathbb{R}$. We optimize this map component over its coefficients c by minimizing the Kullback-Leibler divergence between the target distribution π_j, presumed to be known only through samples, and the map's approximation to the target π_j, which is obtained by applying the inverse map to the standard Gaussian reference η. The resulting objective function $\mathcal{J}$ is (Spantini et al., 2017):

$$\mathcal{J}(S_2) = \sum_{i=1}^{n_{training}} \left(\frac{1}{2}\left(S_2(d^c_{i,j}, h^c_{i,j})\right)^2 - \log \frac{\partial S_2(d^c_{i,1}, h^c_{i,j})}{\partial h^c_{i,j}} \right) \tag{4}$$

The key property of triangular transport maps that allows us to sample conditionals of π_j is that they factorize the target distribution according to the ordering of the variables in Equation 3. While the *forward* map components S_1 and S_2 can be evaluated independently, their *inverses* must be evaluated in sequence:

$$\mathbf{S}^{-1}\left(\mathbf{z}\right) = \begin{bmatrix} S_1^{-1}\left(z_1\right) \\ S_2^{-2}\left(d^c_{:,j}, z_2\right) \end{bmatrix} = \begin{bmatrix} d^c_{:,j} \\ h^c_{:,j} \end{bmatrix} \tag{5}$$

where the inverse of the second map component S_2^{-2} depends on the outcome of the first inversion S_1^{-2}, hence its sequential nature. This effectively factorizes the target distribution as $\pi_j\left(d^c_{:,j}, h^c_{:,j}\right) = \pi_j\left(d^c_{:,j}\right)\pi_j\left(h^c_{:,j}|d^c_{:,j}\right)$, where the second term on the right-hand side is sampled by the inverse S_2^{-1}.

This means that we can sample conditionals of π_j by simply replacing the argument $d^c_{:,j}$ with any values on which we want to condition. Supplying duplicates of the observation $d^c_{obs,j}\mathbf{1}^\top$, where $\mathbf{1}$ is a column vector of 1s, we can sample the desired conditional $\pi_j\left(h^c_{i,j}|d^c_{obs,j}\right)$:

$$\mathbf{t}^{c,\text{cond.}}_{:,j} = S_2^{-1}\left(z_2; d^c_{obs,j}\mathbf{1}^\top\right) \sim \pi_j\left(h^c_{i,j}|d^c_{obs,j}\right) \tag{6}$$

where the required reference samples z_2 can be either drawn from a standard Gaussian distribution, or (better) obtained from the forward map $z_2 = S_2\left(d^c_{:,j}, h^c_{:,j}\right)$. With the conditioned samples $\mathbf{t}^{c,\text{cond.}}_{:,j}$ for each pair of covariates $\left(d^c_{:,j}, h^c_{:,j}\right)$, we can then back-transform the posterior samples into the original target space by ascending from CCA, PCA, and undoing any transformations.

2.4 Experimental design

BEL can be used to assess the amount of information delivered by various data sources. The actual data can have any value within the prior data space, and data sources can be placed anywhere across the grid. To identify highly informative data sets based on their location, one data-utility function must be maximized or minimized (Thibaut et al., 2021). To restrict computation time and keep some realism, we will only consider four well positions around the injection well, which is sufficient to demonstrate the approach. With the geophysical data, a total of 31 different combinations of data sets are possible. These unique combinations are combined with a total of 50 unknown ground truths (test set). Each sample of the test set is sampled with 500 posterior samples. This number is arbitrarily chosen to be high enough to ensure that the posterior distribution is reasonably well-sampled while remaining low enough to keep the computation time manageable. We end up with an array of shape (31, 50, $n_{samples}$, δ) = (number of combinations, test set size, sample set size, number of canonical components).

We use the principal components to perform ED, which is a novel approach in this context. The true target is transformed to the PC space and its RMSE with the predicted targets' PCs is computed. The advantage of working in a lower dimension is that we need to predict a smaller number of dimensions, which is computationally faster. It is easy to show that the prediction error is minimized if the distance between the PCs of the predicted and the observed targets is minimized too, because the back-transformation from the PCs to the observation targets is a linear operation. The minimization of the target prediction error is therefore equivalent to the minimization of the distance between the PCs of the predicted and the observed targets, but is less sensitive to the sample size because of its lower dimension. The PCs are weighted by their explained variance ratio during distance computation because they account for the different importance of the different components. The ED is equivalent to the minimization of the average distances between the PCs of the predicted and observed targets. This is a computationally efficient way to find the optimal well combination, and it has the advantage of being able to consider the different importance of the different variates (through the explained variances). This methodology allows to sort each well combination as a function of the distance to the ideal distribution. We validate our approach wit k-fold cross validation. We repeat our computations across 5 folds (with 5 different seeds) and average the metric results. Averaging across folds is not strictly necessary but will be used here to increase the robustness of the ED. One of the challenges of our case study is the high dimensionality of the problem. This is why using PCs is a great advantage because we can work in a lower dimensional space that contains all of the necessary information. The methodology is summarized below:

Input: training set (D_{train}, H_{train}), test set (D_{test}, H_{test}), data utility function UF
Output: Averaged cross-validation rankings
for all Fold f in 5-fold cross-validation **do**
  $H_{train,f} \leftarrow$ Target training data for fold f
  $H_{train,f} \leftarrow PCA_h.fit\_transform(H_{train,f})$
  $H_{test,f} \leftarrow$ Target test data for fold f
  $H_{test,f} \leftarrow PCA_h.transform(H_{test,f})$
  for all Possible Combinations **do**
    $O \leftarrow Combination$
    $D_{train,f,O} \leftarrow$ Predictor training data for fold f and combination O

$D_{train,f,O} \leftarrow PCA_d.fit\_transform(D_{train,f,O})$
$D_{test,f,O} \leftarrow$ Predictor test data for fold f and combination O
$D_{test,f,O} \leftarrow PCA_d.transform(D_{test,f,O})$
$TrainedModel \leftarrow CCA.fit(D_{train,f,O}, H_{train,f})$ ▷ Training step
for all Ground Truths in $(D_{test,f,O}, H_{test,f})$ **do**
$D_{true} \leftarrow$ True predictor
$D_{true} \leftarrow PCA_d.transform(D_{true})$
$H_{true} \leftarrow$ True target
$H_{true} \leftarrow PCA_h.transform(H_{true})$
$H_{posterior} \leftarrow TrainedModel.predict(D_{true})$ ▷ Predicting in PC space
$Utility \leftarrow UF(H_{posterior}, H_{true})$
$Results.add(Utility)$
end for
$Ranking \leftarrow add(Results)$
$Results.clear()$
end for
end for
$Final \leftarrow mean(Ranking)$

3 Application

3.1 Target prediction

This section shows how to predict a single four-dimensional temperature field, using three distinct predictors: (i) the geophysical data, made of resistance measurements from 1948 quadrupoles over 106 observation time steps, which are combined to form the predictor, (ii) a single temperature profile over 106 observation times, and (iii) the combination of the geophysical data with all (4) borehole temperature curves. We show that BEL can accurately estimate the target posterior distribution with varying uncertainty levels according to the type of predictor used. The dataset in this section has a total size of $n = 250$. The training set is then reduced to $n_{80\%} = 200$ models, with the remaining models being used to validate BEL's ability to predict the target, and later on for ED. Previous BEL applications have demonstrated that making accurate predictions with a dataset of this size is possible (Hermans et al., 2016, 2018, 2019; Athens & Caers, 2019; Michel et al., 2020; J. Park & Caers, 2020; Yin et al., 2020; Thibaut et al., 2021). While a small training set size is inevitable due to the time-consuming nature of the simulations, it is sufficient because the prediction is a temperature distribution that varies smoothly in both time and space and results from advection, diffusion, and dispersion processes. Such target is much simpler than the underlying K model. Because BEL is a Bayesian method, which incorporates uncertainty, a large training set size is not necessarily needed, and the method is not overfitting. Furthermore, the use of cross-validation ensures the robustness of the results.

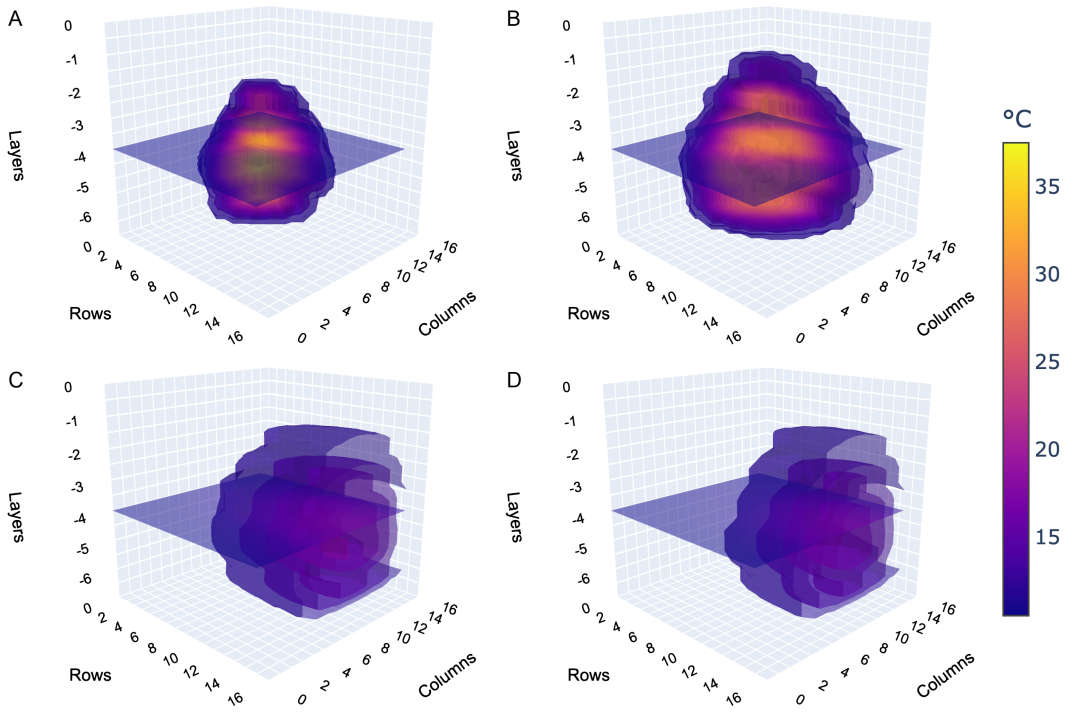

Figure 2. Snapshots of the temperature field at time steps 4 (A), 14 (B), 61 (C) and 74 (D) for one example. The injection well discharge is at (column, row, layer) = (9, 6, -5). The reference plane at the wells level is highlighted.

3.1.1 Pre-processing

The three predictors undergo the pre-processing described in §2.3.1. When geophysical data is combined with borehole temperature curves, the following steps are taken:

1. PCA is performed to explain 99% of the variance in the geophysical data to obtain the PCs $D_{G,99}$
2. The n_b boreholes temperature curves are concatenated into a single array of shape $n_b \times 106$ and then PCA is performed to explain 99% of the variance in the concatenated vector to obtain the PCs $D_{B,99}$
3. The geophysical PCs are concatenated with the borehole temperature curves PCs to obtain the array $D_{G,B,99}$

We have to perform PCA separately for each predictor, because if we simply concatenated the predictor arrays and then applied PCA, the resulting predictor would be more representative of the geophysical data than the borehole temperature curves. Furthermore, the PCs are scaled to unit variance before concatenation because the PCs magnitude can vary greatly from predictor to predictor. The resulting principal components for all cases can directly be compared in Figure 3. The left column shows the predictor PCs, and the right column the target PCs for all cases. For each PC dimension (X-axis), the PC value for each of the 200 training instances is plotted (Y-axis). The example test instance is plotted on top of the training instances. The required number of PCs is chosen to account for 99 percent of the variance in the predictor. In parallel, PCA is applied to the target. In line with our methodology, the number of components to keep is set to the maximum number of PCs required by the predictor, and the corresponding amount of variance explained in the target is summarized in Table 2.

Parameter \Combination	**G**	**1**	1, 2	1, 2, 3	1, 2, 3, 4	**G, 1, 2, 3, 4**
δ	10	3	6	9	11	21
Explained variance (target)	77%	57%	69%	75%	78%	87%

Table 2. Effect of the number of PCs on the target PCA. **G** stands for geophysical data. **1, 2, 3, 4** stand for the borehole temperature curves. Case (i) is **G**, case (ii) is **1** and case (iii) is **G, 1, 2, 3, 4**

When a single temperature profile is used as a predictor (Case (ii)), the target variance is not explained as well as when the entire set of predictor data is used (Case (iii)), hence the smaller number of target PCs required. When the predictor is a combination of geophysical data and all temperature profiles, some additional variance is captured. The remaining target PCs for each case are shown in Figure 3B, D and C. These additional target components are not used in training. They are, however, saved for subsequent use in ED.

3.1.2 Training and prediction

The CCA mapping allows the fusion of the low-dimensional representation of the predictor with the low-dimensional representation of the target in order to make predictions of the target distribution. It is run on all cases to find the canonical variates that define the relation between the predictor and the target, using a maximum of 21 PCs on the predictor. The first three canonical variate pairs for each case are shown in Figure 4. Each row corresponds to a single case, and each column to a single canonical variate pair. The variable ρ is the correlation between the canonical variates, and can be interpreted as the amount of mutual information shared between the target and predictor. For all cases, the predictor explains a large part of the target: ρ_1 (first pair) = 0.998, 0.962 and 1 for case (i), (ii) and (iii) respectively. Hence, CCA is well-suited for our purposes. The canonical variates for case (ii) provide a poorer explanation for the target (ρ_2 (second pair) = 0.297), giving the impression that the temperature profiles do not help greatly in the prediction of the target, whereas the case (iii) show that they do, to a certain extent, which makes sense given that the temperature curves used as predictors are simply one-dimensional and only convey information about a small part of our model over time. The strong correlations in the canonical variates pairs of cases (i) and (iii) is further indication of the suitability of CCA for this study. Transport map inference is run for each pair for each case, using the test predictor (on the X-axis (d^c) of Figure 4). The 500 samples of $p(h^c|d^c_*)$ in Figure 4 represent our predictions of the unknown target distribution in the canonical space. They can then be sequentially back-transformed to the principal component space (see posterior samples in Figure 3) and to the original space (see Figures 5 and 6 for 1D and 2D representations, respectively).

Figure 5 shows the temperature curves of the 500 samples at the location of the observation well number 2 for each case. This point was arbitrarily chosen to illustrate the one-dimensional temperature curve at one observation point. Across cases, the level of uncertainty, expressed by the spread of the temperature curves, is higher during the injection and storage phases than it is during the pumping phase, which is a positive development because this portion of the curve is the part that is typically inferred for ATES systems (energy recovery). The magnitude of the spread of the predicted samples in the canonical space (Figure 4) is sequentially transmitted through the principal component space (Figure 3) and the original space (Figure 5), since the data flows through linear transformations.

On Figure 6A, the true (test) temperature cross-section at layer 9 (at a depth of 4.5m) and time t=105.75h (pumping phase) is shown. Figure 6B shows one randomly drawn example from the 500 sampled temperature profiles when using the ERT predictor alone. The results are not only visually close to the truth, but the absolute temperature difference ranges from -0.8 to 0.4 degrees Celsius, which is the magnitude of accuracy we expect when using resistance data (Hermans et al., 2015). Figures 6C and 6D show the same results when a single borehole temperature profile and the full combination of ERT and temperature profiles are used, respectively. The single borehole image is the least accurate, while the combination of all temperature profiles and ERT is the most accurate. This is to be expected; a single borehole temperature profile provides data for a small fraction of the volume, whereas combining all temperature profiles provides more information. Although it appears that the single borehole temperature profile has no effect on the ERT predictor's accuracy, we must remember that we are only looking at a 2D image of the temperature field from a random sample. The information gain must be assessed by comparing Figures 5B and C rather than Figures 6C and D.

Because the underlying internal behavior of the aquifer is nonlinear, given the number of parameters involved, the underlying physics of the model and the nature of the predictor (indirect geophysical data), such a level of uncertainty is expected (Hermans et al., 2015, 2016, 2018). Considering the level of complexity of the underlying physics and the relatively small training set, BEL is capable of inferring different possible outcomes with reasonable uncertainty.

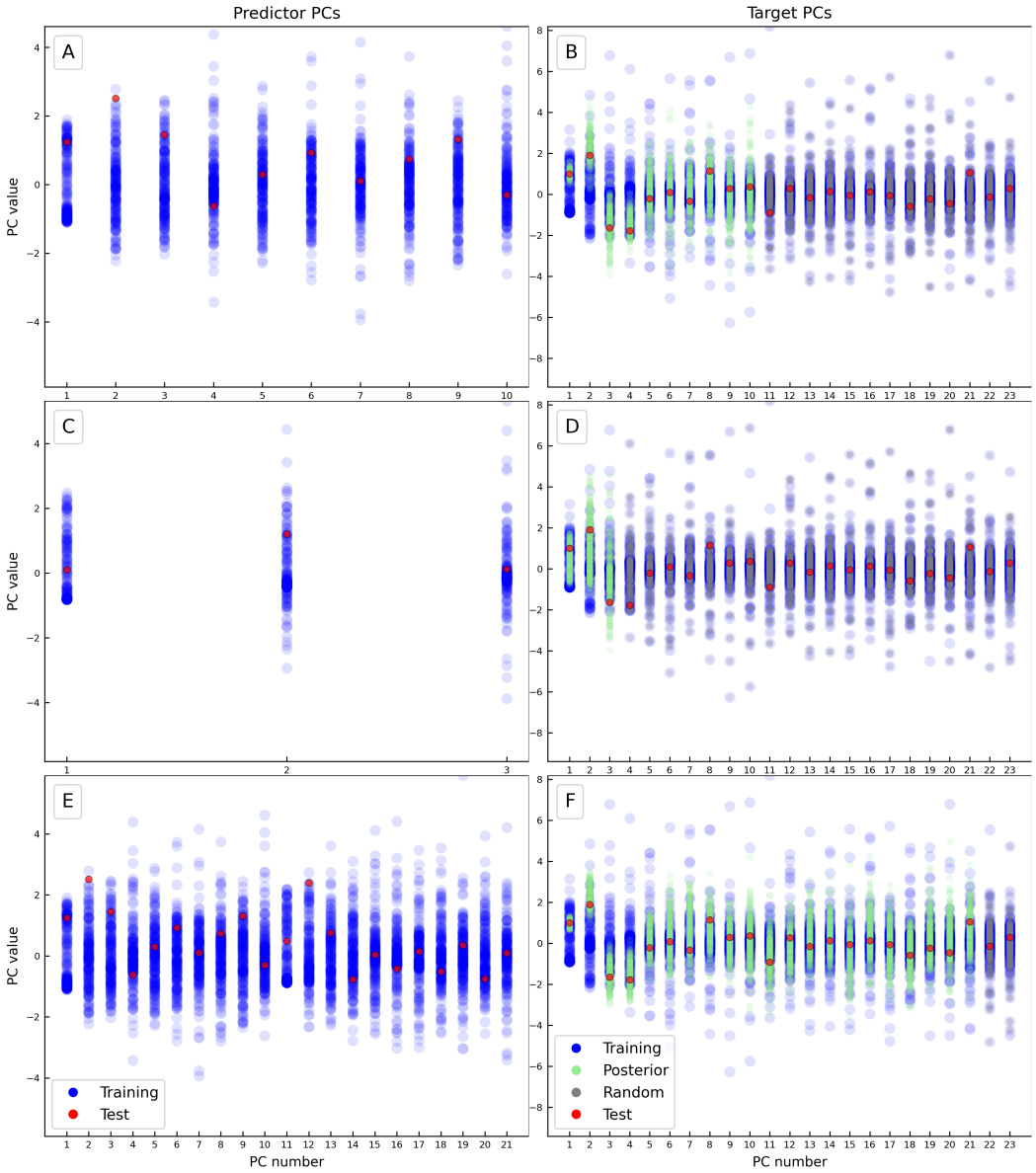

Figure 3. Principal Component Scores. The 'Random' PC samples are drawn at random from the target PC training set. They will be used in the ED section 4. A. Case (i). Predictor: ERT data, B. Case (i). Target. C. Case (ii). Predictor: Temperature profile from borehole 1. D. Case (ii). Target. E. Case (iii). Predictor: Full combination (ERT data + four boreholes temperature profiles). F. Case (iii). Target.

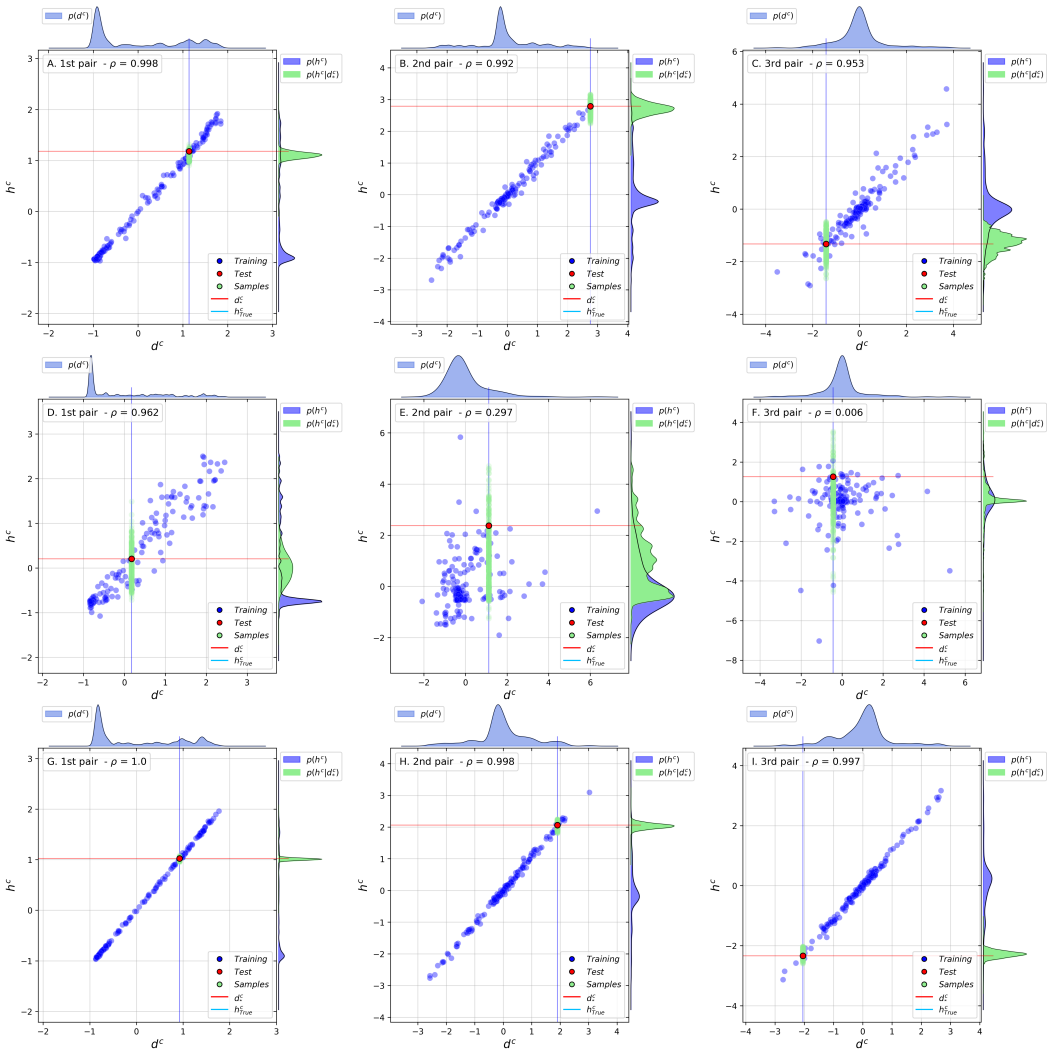

Figure 4. Canonical Variate Pairs (1 to 3). The first row (A, B, C), case (i): uses the geophysical predictor, the second row (D, E, F), case (ii): uses the borehole predictor, and the third row (G, H, I), case (iii): uses both predictors. The true point coordinates (Test) are highlighted by the two lines in each dimension.

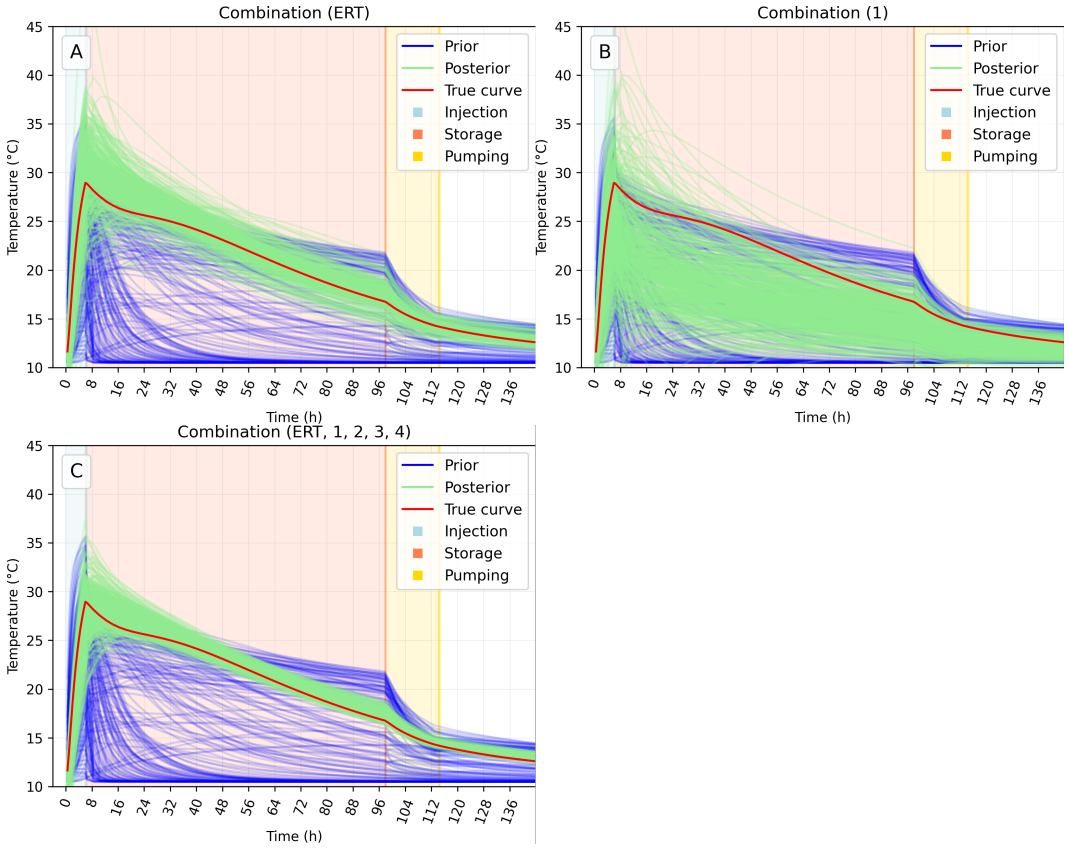

Figure 5. Temperature curves across all time steps, at the observation well 4. A. Using the ERT as predictor. B. Using the temperature curves at well 1 as predictor. C. Using the ERT and all the temperature curves at wells 1, 2, 3 and 4 as predictors.

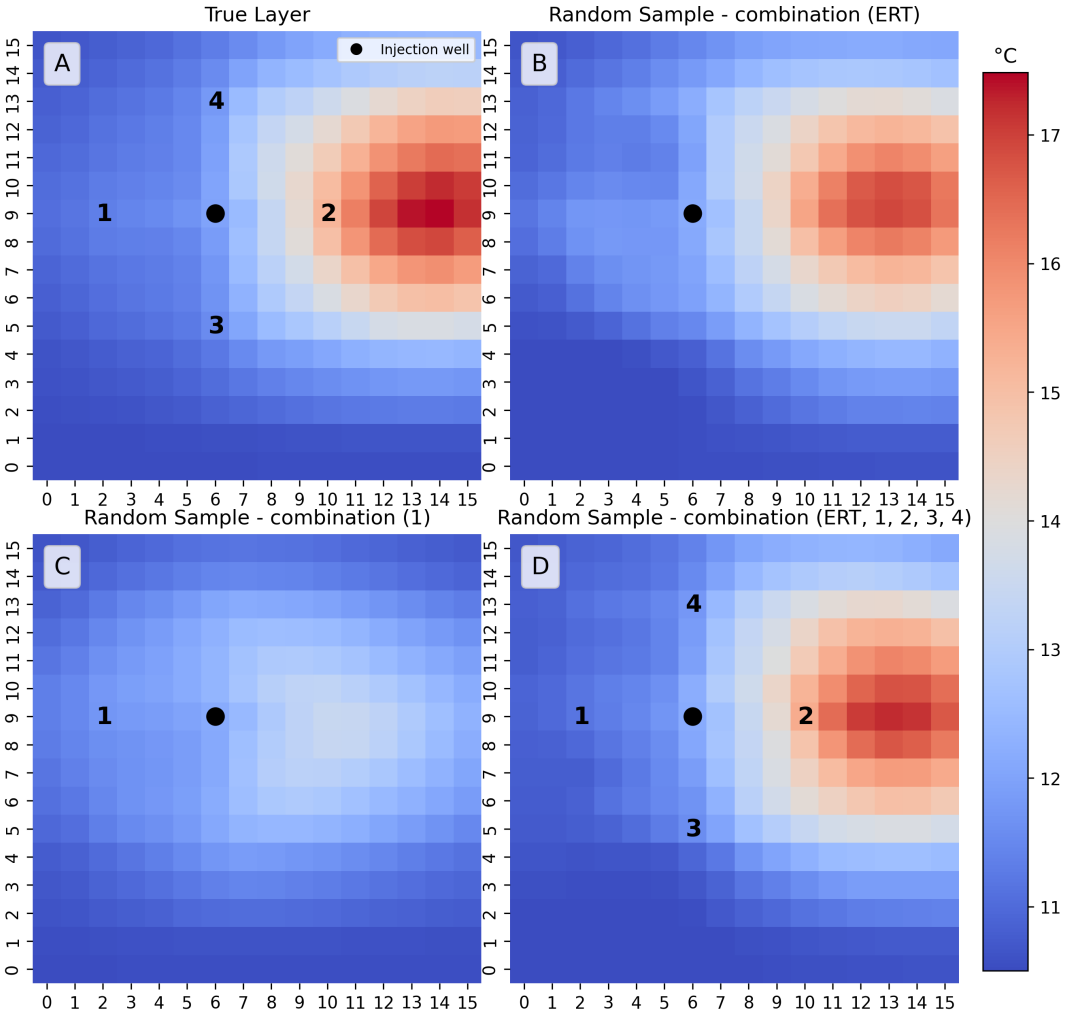

Figure 6. Cross-section of the temperature field at time step 74 (105.75 hours - pumping phase) and layer 9. A. Ground truth. B. Using the ERT as predictor. C. Using the temperature curves at well 1 as predictor. D. Using the ERT and all the temperature curves at wells 1, 2, 3 and 4 as predictors.

4 Results and discussion

Random components from the training set are chosen for ED, as shown in Figure 3. The extra random components, which were not used for training, could thus not be predicted, but they must be included for experimental design purposes. The goal is to obtain the same number of components in each case so that the different methods can be compared fairly. Without them, the prediction performance would be biased. They must be selected at random for each PC dimension in order to avoid bias in the results. It ensures that the score of the combination will be representative of the actual prediction performance.

The expected outcome is a ranking of combinations ranging from a small number of combinations to all considered data sources, with the most unfavourable case being the use of a single observation well and the most favourable case being the use of geophysical data and all available wells, as can be visually evaluated across cases on Figure 5.

To derive a robust ED, we average the results over the test set of ground truth models. However, the results depend on the chosen ground truth models set, so a combination that is ranked as the best in one case may not be ranked as such for another set, which is why we use a 5-fold cross-validation to validate our findings. We use k-fold cross-validation to produce predictions over 5 different training and test sets. We average the rankings across folds to obtain the final ranking. Figure 7A to E depicts the results of all 31 combinations over the 5 folds. Figure 7F is the average of these results. The geophysical data is labeled as 'G' and the well data are labeled by their well ID (1, 2, 3, 4). For example, 'G12' is the combination of geophysical data with wells 1 and 2. The results are consistent with what was expected, and using more data sources (labeled as '*ds*' in Figure 7) yields the best results, which is logical given the symmetry of our observation wells network. Our findings show that the ERT data alone provides the most information to the model, with a clear difference between the wells alone and the ERT data. To demonstrate that there is no overlap between the two, a darker background colour indicates when the ERT data is used, and a lighter background colour indicates when the wells alone are used. Our findings support previous findings that ERT is a valuable tool for monitoring the development of thermally affected zones in aquifers (Lesparre et al., 2019; Hermans et al., 2016).

In terms of observation wells, wells 1 and 4 are consistently ranked as the least favorable cases. Well 3 is ranked in the middle, while well 2 is consistently ranked as the best case. This is due to the direction of the heat plume over time. As shown on Figures 2, 5 and 6, the gradient causes the plume to move in the direction of downstream well 2, allowing well 2 to record more variation from the plume over time. However, because the plume is moving away from them, wells 1, 3, and 4 are more likely to record redundant data from it (e.g., a flat temperature curve), which makes them less relevant for development of the model.

Similar observations were made in the case of solute transport in Thibaut et al. (2021): downstream wells provided the most useful data. In their settings, their tracer curves provided more information on their underlying K field, lowering their prediction's uncertainty. They did not investigate the information gained from any geophysical data, which in our case is sufficient to understand the evolution of the heat plume, but it is important to note that the overall information gain from the combination of all wells and ERT is the highest. Since ERT is an indirect data source, adding at least one borehole allows to provide direct information on the temperature and thus to reduce the uncertainty.

To corroborate our findings, we reproduce the experiment using four different wells, but with the same data (the previous k-fold shuffle seed was saved). The positions of the wells are shown in Figure 8A and the results are shown in Figure 8B. The outcomes are in line with expectations. The worst-case scenario is well number 3. It is located upstream and is less affected by the heat plume. Because of its proximity to the injection well, well number 1 is the best case. The combination of the various wells produces more insightful results than before. Wells 2 and 4 are located downstream and away from the injection well. They collect more data from the heat plume as a group than other observation wells. In fact, while well 1 is ranked higher, the combination of wells 2 and 4 ('24' on Figure 8) provides the most information when compared to the combinations of well 1 and well 2 ('12' and '14' on Figure 8). Following the same logic, the combination of wells 1, 2, and 4 ('124') is the best case, as expected. The increase in information provided by geophysical data is not as strong as in the previous case.

It was also expected, since the four observation wells in the previous case were symmetrically placed around the injection well, and the information provided over time was more redundant. The location of the well in relation to the plume appears to have a large influence on the information content of the well.

A fundamental question is how we will put our framework into action in order to make the best decisions. Testing for all well positions and combinations is possible in our synthetic study, but time-consuming, because each combination requires a training and testing phase. As a reminder, the number of possible combinations is $\frac{n!}{w!(n-w)!}$, where n is the number of possible positions and w is the number of wells. For a number of 3 wells and 256 possible positions (number of cells for one plane in the grid), the number of possible combinations is $2,763,520$. Nevertheless, it is based on the same 250 heat flow and transport simulations, so the most expensive part is not repeated. As a result, running the experimental design for a representative subset of these combinations is feasible. Constraints such as at least 5 m between wells, at least one well upstream and one downstream, and so on can be used to reduce the number of possible combinations.

One ideal situation in which to apply our framework is when potential well locations are predetermined and limited by factors such as land occupation. The situation where the wells are already positioned, and we are looking for the single next-best well position is an alternative ideal situation. However, this topic is beyond the scope of this contribution. Future research will investigate the ability of the framework to select new sensor measurements, and solve the problem of allocating new expensive drill-core samples iteratively such as, e.g., Haan et al. (2021).

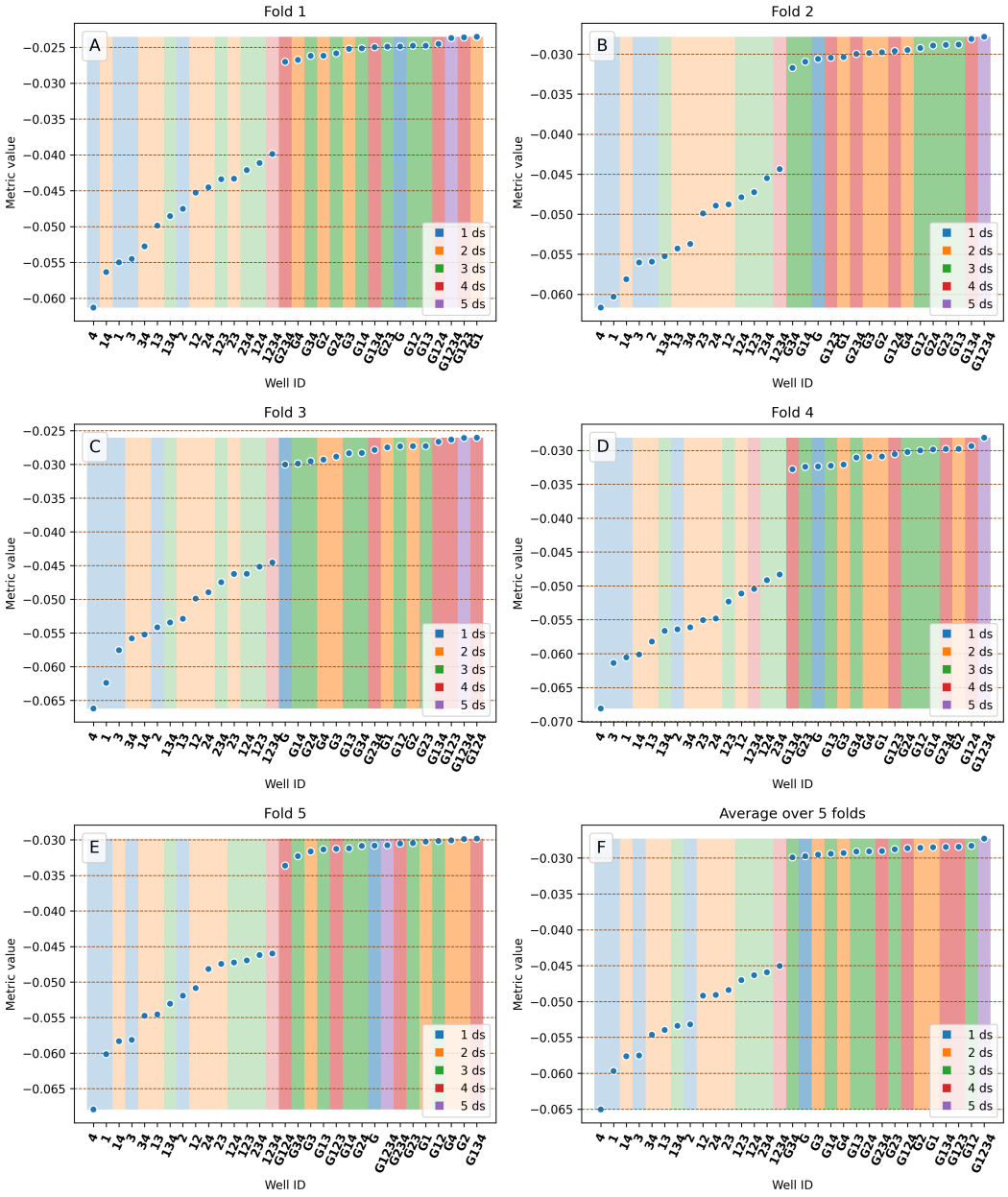

Figure 7. Ranking of the different combinations of data sources ('**ds**'). To visualize a higher score for the best combination, the metric (RMSE) values opposite are displayed. The use of ERT data is indicated by a darker background shade, whereas the use of wells alone is indicated by a lighter shade. A. Fold 1. B. Fold 2. C. Fold 3. D. Fold 4. E. Fold 5. F. Average of all folds.

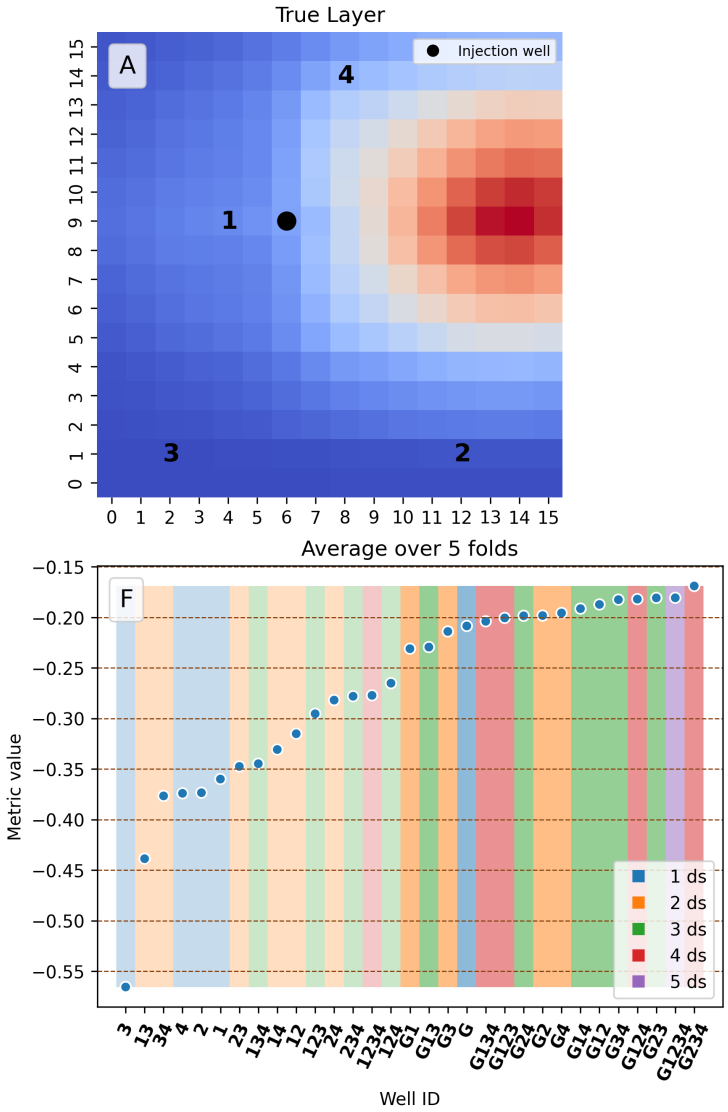

Figure 8. Alternative well locations. Ranking of the different combinations of data sources ('**ds**'). To visualize a higher score for the best combination, the metric (RMSE) values opposite are displayed. The use of ERT data is indicated by a darker background shade, whereas the use of wells alone is indicated by a lighter shade. A. Well locations. B. Ranking of the different combinations of data sources.

5 Conclusion

In this paper, we present a method for optimizing 4D temperature field monitoring experiments using a Bayesian approach. The proposed methodology uses a combination of ED and Bayesian inference to identify informative observation wells locations. We apply our method to a synthetic case study involving the prediction of a four-dimensional temperature field from data collected by electrical resistivity tomography (ERT) and four observation wells. These predictors of different nature are combined in the principal component space to form a new predictor. Following the training step, targets are sampled from the inferred posterior distribution using transport map methods, which are a powerful tool in our Bayesian inference framework for sampling an unknown target given a

known predictor. Applying a simple metric (RMSE) to the principal components of the predicted and true targets allows to determine the locations of observation wells that minimize uncertainty. This method can be used to optimize the design of 4D temperature field monitoring experiments and to reduce the cost of data collection by choosing a threshold between precision and number and nature of the data.

Our findings suggest that the placement of observation wells must take into account the direction of the heat plume, and that the optimal case is to have observation wells that are downstream from the original injection well (in the direction of the plume). A combination of various observation wells and geophysical data always yields the best results. Given the available data, this approach is a good method for determining the best combination of observations to use to predict the target.

One of the limitations of this method is that it requires a training set of data. This can be difficult to obtain, because it requires knowledge of the prior distribution of the model parameters, and their simulation is computationally expensive. However, with a small number of examples (250 in our study) the method is able to predict the posterior distribution of the temperature field with a reasonable accuracy and to find the best combination of data sources among four prescribed well positions and their combinations, with the caveat that the training set should be as representative as possible of the real data. It is also important to note that the proposed method is not limited to the prediction of temperature fields and can be applied to the prediction of any type of high-dimensional target.

6 Open Research

The software developments related to this paper are distributed in the software SKBEL (v2.0.0) published on GitHub under the BSD 3-Clause License (Thibaut & Ramgraber, 2021). Additionally, the dataset is available on Kaggle (Lesparre et al., 2022) under the terms of the CC BY-SA 4.0 License. It includes the data used in the paper (Temperature field monitoring with ERT data) and Jupyter notebooks to reproduce the results.

References

Arato, A., Boaga, J., Comina, C., Seta, M. D., Sipio, E. D., Galgaro, A., ... Mandrone, G. (2015, 8). Geophysical monitoring for shallow geothermal applications – two italian case histories. *First Break*, *33*. Retrieved from https://www.earthdoc.org/content/journals/0.3997/1365-2397.33.8.82010 doi: 10.3997/1365-2397.33.8.82010

Asher, M. J., Croke, B. F. W., Jakeman, A. J., & Peeters, L. J. M. (2015, 8). A review of surrogate models and their application to groundwater modeling. *Water Resources Research*, *51*, 5957-5973. Retrieved from http://doi.wiley.com/10.1002/2015WR016967 doi: 10.1002/2015WR016967

Athens, N. D., & Caers, J. K. (2019, 12). A monte carlo-based framework for assessing the value of information and development risk in geothermal exploration. *Applied Energy*, *256*, 113932. Retrieved from https://linkinghub.elsevier.com/retrieve/pii/S0306261919316198 doi: 10.1016/j.apenergy.2019.113932

Babaei, M., Pan, I., & Alkhatib, A. (2015, 12). Robust optimization of well location to enhance hysteretical trapping of co ¡sub¿2¡/sub¿ : Assessment of various uncertainty quantification methods and utilization of mixed response surface surrogates. *Water Resources Research*, *51*, 9402-9424. Retrieved from http://doi.wiley.com/10.1002/2015WR017418 doi: 10.1002/2015WR017418

Bayer, P., Rybach, L., Blum, P., & Brauchler, R. (2013, 10). Review on life cycle environmental effects of geothermal power generation. *Renewable and Sustainable*

Energy Reviews, *26*, 446-463. Retrieved from https://linkinghub.elsevier.com/retrieve/pii/S1364032113003420 doi: 10.1016/j.rser.2013.05.039

Bridger, D. W., & Allen, D. M. (2010, 1). Heat transport simulations in a heterogeneous aquifer used for aquifer thermal energy storage (ates). *Canadian Geotechnical Journal*, *47*, 96-115. Retrieved from http://www.nrcresearchpress.com/doi/10.1139/T09-078 doi: 10.1139/T09-078

Brouyère, S. (2001). *Etude et modélisation du transport et du piégeage des solutés en milieu souterrain variablement saturé (study and modelling of transport and retardation of solutes in variably saturated media).* (PhD thesis ed.). Retrieved from https://hdl.handle.net/2268/40804

Brunner, P., & Simmons, C. T. (2012, 3). Hydrogeosphere: A fully integrated, physically based hydrological model. *Ground Water*, *50*, 170-176. doi: 10.1111/j.1745-6584.2011.00882.x

Dassargues, A. (1997, 3). Modeling baseflow from an alluvial aquifer using hydraulic-conductivity data obtained from a derived relation with apparent electrical resistivity. *Hydrogeology Journal*, *5*, 97-108. Retrieved from http://link.springer.com/10.1007/s100400050125 doi: 10.1007/s100400050125

de Barros, F. P., Ezzedine, S., & Rubin, Y. (2012, February). Impact of hydrogeological data on measures of uncertainty, site characterization and environmental performance metrics. *Advances in Water Resources*, *36*, 51–63. Retrieved 2021-02-05, from https://linkinghub.elsevier.com/retrieve/pii/S0309170811000959 doi: 10.1016/j.advwatres.2011.05.004

Derouane, J., & Dassargues, A. (1998, 11). Delineation of groundwater protection zones based on tracer tests and transport modeling in alluvial sediments. *Environmental Geology*, *36*, 27-36. Retrieved from http://link.springer.com/10.1007/s002540050317 doi: 10.1007/s002540050317

Duijff, R., Bloemendal, M., & Bakker, M. (2021, 12). Interaction effects between aquifer thermal energy storage systems. *Groundwater*, gwat.13163. Retrieved from https://onlinelibrary.wiley.com/doi/10.1111/gwat.13163 doi: 10.1111/gwat.13163

El Moselhy, T. A., & Marzouk, Y. M. (2012, October). Bayesian inference with optimal maps. *Journal of Computational Physics*, *231*(23), 7815–7850. Retrieved 2022-03-01, from https://linkinghub.elsevier.com/retrieve/pii/S0021999112003956 doi: 10.1016/j.jcp.2012.07.022

Ferguson, G. (2007, 7). Heterogeneity and thermal modeling of ground water. *Ground Water*, *45*, 485-490. Retrieved from https://onlinelibrary.wiley.com/doi/10.1111/j.1745-6584.2007.00323.x doi: 10.1111/j.1745-6584.2007.00323.x

Goovaerts, P. (1997). *Geostatistics for natural resources evaluation.* New York: Oxford University Press.

Haan, S., Ramos, F., & Müller, R. D. (2021, 1). Multiobjective bayesian optimization and joint inversion for active sensor fusion. *Geophysics*, *86*, ID1-ID17. Retrieved from https://library.seg.org/doi/10.1190/geo2019-0460.1 doi: 10.1190/geo2019-0460.1

Hermans, T., Lesparre, N., De Schepper, G., & Robert, T. (2019, August). Bayesian evidential learning: a field validation using push-pull tests. *Hydrogeology Journal*, *27*(5), 1661–1672. Retrieved 2020-11-21, from http://link.springer.com/10.1007/s10040-019-01962-9 doi: 10.1007/s10040-019-01962-9

Hermans, T., Nguyen, F., Klepikova, M., Dassargues, A., & Caers, J. (2018, 1). Uncertainty quantification of medium-term heat storage from short-term geophysical experiments using bayesian evidential learning. *Water Resources Research*, *54*, 2931-2948. doi: 10.1002/2017WR022135

Hermans, T., Nguyen, F., Robert, T., & Revil, A. (2014, 8). Geophysical methods for monitoring temperature changes in shallow low enthalpy geothermal systems. *Energies*, *7*, 5083-5118. Retrieved from http://www.mdpi.com/

1996-1073/7/8/5083 doi: 10.3390/en7085083

Hermans, T., Oware, E., & Caers, J. (2016, 9). Direct prediction of spatially and temporally varying physical properties from time-lapse electrical resistance data. *Water Resources Research*, *52*, 7262-7283. Retrieved from http://doi.wiley.com/10.1002/2016WR019126 doi: 10.1002/2016WR019126

Hermans, T., Vandenbohede, A., Lebbe, L., & Nguyen, F. (2012, 1). A shallow geothermal experiment in a sandy aquifer monitored using electric resistivity tomography. *GEOPHYSICS*, *77*, B11-B21. Retrieved from https://library.seg.org/doi/10.1190/geo2011-0199.1 doi: 10.1190/geo2011-0199.1

Hermans, T., Wildemeersch, S., Jamin, P., Orban, P., Brouyère, S., Dassargues, A., & Nguyen, F. (2015, 1). Quantitative temperature monitoring of a heat tracing experiment using cross-borehole ert. *Geothermics*, *53*, 14-26. Retrieved from https://linkinghub.elsevier.com/retrieve/pii/S0375650514000376 doi: 10.1016/j.geothermics.2014.03.013

Kikuchi, C. P., Ferré, T. P. A., & Vrugt, J. A. (2015, 6). On the optimal design of experiments for conceptual and predictive discrimination of hydrologic system models. *Water Resources Research*, *51*, 4454-4481. Retrieved from http://doi.wiley.com/10.1002/2014WR016795 doi: 10.1002/2014WR016795

Klepikova, M. V., Borgne, T. L., Bour, O., Dentz, M., Hochreutener, R., & Lavenant, N. (2016, 7). Heat as a tracer for understanding transport processes in fractured media: Theory and field assessment from multiscale thermal push-pull tracer tests. *Water Resources Research*, *52*, 5442-5457. Retrieved from http://doi.wiley.com/10.1002/2016WR018789 doi: 10.1002/2016WR018789

Laloy, E., Rogiers, B., Vrugt, J. A., Mallants, D., & Jacques, D. (2013, 5). Efficient posterior exploration of a high-dimensional groundwater model from two-stage markov chain monte carlo simulation and polynomial chaos expansion. *Water Resources Research*, *49*, 2664-2682. Retrieved from http://doi.wiley.com/10.1002/wrcr.20226 doi: 10.1002/wrcr.20226

Laloy, E., & Vrugt, J. A. (2012, jan). High-dimensional posterior exploration of hydrologic models using multiple-try DREAM (ZS) and high-performance computing. *Water Resources Research*, *48*(1). Retrieved from http://doi.wiley.com/10.1029/2011WR010608 doi: 10.1029/2011WR010608

Lesparre, N., Compaire, N., Hermans, T., & Thibaut, R. (2022). *4D temperature monitoring* [Dataset]. Kaggle. Retrieved from https://www.kaggle.com/dsv/3819983 doi: 10.34740/kaggle/dsv/3819983

Lesparre, N., Robert, T., Nguyen, F., Boyle, A., & Hermans, T. (2019, 1). 4d electrical resistivity tomography (ert) for aquifer thermal energy storage monitoring. *Geothermics*, *77*, 368-382. Retrieved from https://linkinghub.elsevier.com/retrieve/pii/S0375650517303772 doi: 10.1016/j.geothermics.2018.10.011

Leube, P. C., Geiges, A., & Nowak, W. (2012, 2). Bayesian assessment of the expected data impact on prediction confidence in optimal sampling design. *Water Resources Research*, *48*. Retrieved from http://doi.wiley.com/10.1029/2010WR010137 doi: 10.1029/2010WR010137

Linde, N., Ginsbourger, D., Irving, J., Nobile, F., & Doucet, A. (2017, December). On uncertainty quantification in hydrogeology and hydrogeophysics. *Advances in Water Resources*, *110*, 166–181. Retrieved 2021-02-05, from https://linkinghub.elsevier.com/retrieve/pii/S0309170817304608 doi: 10.1016/j.advwatres.2017.10.014

Macfarlane, A., Förster, A., Merriam, D., Schrötter, J., & Healey, J. (2002, 12). Monitoring artificially stimulated fluid movement in the cretaceous dakota aquifer, western kansas. *Hydrogeology Journal*, *10*, 662-673. Retrieved from http://link.springer.com/10.1007/s10040-002-0223-7 doi:

10.1007/s10040-002-0223-7

Meloun, M., & Militký, J. (Eds.). (2012). *Statistical data analysis: a practical guide* (Reprinted ed.). New Delhi: WPI, Woodhead Publ. India Pvt. Ltd. (OCLC: 696087077)

Michel, H., Hermans, T., & Nguyen, F. (2022, 9). Iterative prior resampling and rejection sampling to improve 1d geophysical imaging based on bayesian evidential learning (bel1d). *Geophysical Journal International*. doi: 10.1093/gji/ggac372

Michel, H., Nguyen, F., Kremer, T., Elen, A., & Hermans, T. (2020, 5). 1d geological imaging of the subsurface from geophysical data with bayesian evidential learning. *Computers & Geosciences*, *138*, 104456. Retrieved from https://linkinghub.elsevier.com/retrieve/pii/S0098300419306028 doi: 10.1016/j.cageo.2020.104456

Neuman, S. P., Xue, L., Ye, M., & Lu, D. (2012, 2). Bayesian analysis of data-worth considering model and parameter uncertainties. *Advances in Water Resources*, *36*, 75-85. Retrieved from https://linkinghub.elsevier.com/retrieve/pii/S0309170811000339 doi: 10.1016/j.advwatres.2011.02.007

Palmer, C. D., Blowes, D. W., Frind, E. O., & Molson, J. W. (1992, 10). Thermal energy storage in an unconfined aquifer: 1. field injection experiment. *Water Resources Research*, *28*, 2845-2856. Retrieved from http://doi.wiley.com/10.1029/92WR01471 doi: 10.1029/92WR01471

Park, B.-H., Bae, G.-O., & Lee, K.-K. (2015, 11). Importance of thermal dispersivity in designing groundwater heat pump ({GWHP}) system: {Field} and numerical study. *Renewable Energy*, *83*, 270-279. Retrieved from https://linkinghub.elsevier.com/retrieve/pii/S096014811500316X doi: 10.1016/j.renene.2015.04.036

Park, J., & Caers, J. (2020, October). Direct forecasting of global and spatial model parameters from dynamic data. *Computers & Geosciences*, *143*, 104567. Retrieved 2021-01-30, from https://linkinghub.elsevier.com/retrieve/pii/S0098300420305562 doi: 10.1016/j.cageo.2020.104567

Pham, H. V., & Tsai, F. T.-C. (2016, February). Optimal observation network design for conceptual model discrimination and uncertainty reduction: OBSERVATION NETWORK DESIGN FOR MODEL DISCRIMINATION. *Water Resources Research*, *52*(2), 1245–1264. Retrieved 2021-02-04, from http://doi.wiley.com/10.1002/2015WR017474 doi: 10.1002/2015WR017474

Polydorides, N., & Lionheart, W. R. B. (2002, 12). A matlab toolkit for three-dimensional electrical impedance tomography: a contribution to the electrical impedance and diffuse optical reconstruction software project. *Measurement Science and Technology*, *13*, 1871-1883. doi: 10.1088/0957-0233/13/12/310

Pradhan, A., & Mukerji, T. (2020, 6). Seismic bayesian evidential learning: estimation and uncertainty quantification of sub-resolution reservoir properties. *Computational Geosciences*, *24*, 1121-1140. Retrieved from http://link.springer.com/10.1007/s10596-019-09929-1 doi: 10.1007/s10596-019-09929-1

Raftery, A. E., Gneiting, T., Balabdaoui, F., & Polakowski, M. (2005, 5). Using bayesian model averaging to calibrate forecast ensembles. *Monthly Weather Review*, *133*, 1155-1174. Retrieved from http://journals.ametsoc.org/doi/10.1175/MWR2906.1 doi: 10.1175/MWR2906.1

Razavi, S., Tolson, B. A., & Burn, D. H. (2012, 7). Review of surrogate modeling in water resources. *Water Resources Research*, *48*. Retrieved from http://doi.wiley.com/10.1029/2011WR011527 doi: 10.1029/2011WR011527

Robert, Paulus, Bolly, Lin, K. S., & Hermans. (2019, 9). Heat as a proxy to image dynamic processes with 4d electrical resistivity tomography. *Geosciences*, *9*, 414. Retrieved from https://www.mdpi.com/2076-3263/9/10/414 doi: 10.3390/geosciences9100414

Samadi, S., Pourreza-Bilondi, M., Wilson, C. A. M. E., & Hitchcock, D. B. (2020, 7). Bayesian model averaging with fixed and flexible priors: Theory, concepts, and calibration experiments for rainfall-runoff modeling. *Journal of Advances in Modeling Earth Systems*, *12*. Retrieved from https://onlinelibrary.wiley.com/doi/10.1029/2019MS001924 doi: 10.1029/2019MS001924

Saner, D., Juraske, R., Kübert, M., Blum, P., Hellweg, S., & Bayer, P. (2010, 9). Is it only co2 that matters? a life cycle perspective on shallow geothermal systems. *Renewable and Sustainable Energy Reviews*, *14*, 1798-1813. Retrieved from https://linkinghub.elsevier.com/retrieve/pii/S1364032110001061 doi: 10.1016/j.rser.2010.04.002

Satija, A., & Caers, J. (2015, March). Direct forecasting of subsurface flow response from non-linear dynamic data by linear least-squares in canonical functional principal component space. *Advances in Water Resources*, *77*, 69–81. Retrieved 2021-01-30, from https://linkinghub.elsevier.com/retrieve/pii/S0309170815000044 doi: 10.1016/j.advwatres.2015.01.002

Scheidt, C., Li, L., & Caers, J. (2018). *Quantifying Uncertainty in Subsurface Systems*. Hoboken, NJ, USA: John Wiley & Sons, Inc. Retrieved 2020-09-29, from http://doi.wiley.com/10.1002/9781119325888 doi: 10.1002/9781119325888

Scheidt, C., Renard, P., & Caers, J. (2015, February). Prediction-Focused Subsurface Modeling: Investigating the Need for Accuracy in Flow-Based Inverse Modeling. *Mathematical Geosciences*, *47*(2), 173–191. Retrieved 2021-01-30, from http://link.springer.com/10.1007/s11004-014-9521-6 doi: 10.1007/s11004-014-9521-6

Sommer, W., Valstar, J., van Gaans, P., Grotenhuis, T., & Rijnaarts, H. (2013, 12). The impact of aquifer heterogeneity on the performance of aquifer thermal energy storage. *Water Resources Research*, *49*, 8128-8138. Retrieved from http://doi.wiley.com/10.1002/2013WR013677 doi: 10.1002/2013WR013677

Sommer, W. T., Doornenbal, P. J., Drijver, B. C., van Gaans, P. F. M., Leusbrock, I., Grotenhuis, J. T. C., & Rijnaarts, H. H. M. (2014, 2). Thermal performance and heat transport in aquifer thermal energy storage. *Hydrogeology Journal*, *22*, 263-279. Retrieved from http://link.springer.com/10.1007/s10040-013-1066-0 doi: 10.1007/s10040-013-1066-0

Spantini, A., Bigoni, D., & Marzouk, Y. (2017, 3). Inference via low-dimensional couplings. *Journal of Machine Learning Research*, *19*.

Tadjer, A., & Bratvold, R. B. (2021). Managing uncertainty in geological co2 storage using bayesian evidential learning. *Energies*, *14*. doi: 10.3390/en14061557

Tarakanov, A., & Elsheikh, A. H. (2020, October). Optimal bayesian experimental design for subsurface flow problems. *Computer Methods in Applied Mechanics and Engineering*, *370*, 113208. Retrieved 2021-07-14, from https://linkinghub.elsevier.com/retrieve/pii/S0045782520303935 doi: 10.1016/j.cma.2020.113208

Thibaut, R., Laloy, E., & Hermans, T. (2021, 12). A new framework for experimental design using bayesian evidential learning: The case of wellhead protection area. *Journal of Hydrology*, *603*, 126903. Retrieved from https://linkinghub.elsevier.com/retrieve/pii/S0022169421009537 doi: 10.1016/j.jhydrol.2021.126903

Thibaut, R., & Ramgraber, M. (2021, September). *SKBEL - bayesian evidential learning framework built on top of scikit-learn* [Software]. Zenodo. Retrieved from https://doi.org/10.5281/zenodo.6205242 doi: 10.5281/zenodo.6205242

Tsai, F. T.-C., & Li, X. (2008, 9). Inverse groundwater modeling for hydraulic conductivity estimation using bayesian model averaging and variance window.

Water Resources Research, *44*. Retrieved from http://doi.wiley.com/10.1029/2007WR006576 doi: 10.1029/2007WR006576

Vandenbohede, A., Hermans, T., Nguyen, F., & Lebbe, L. (2011, 10). Shallow heat injection and storage experiment: Heat transport simulation and sensitivity analysis. *Journal of Hydrology*, *409*, 262-272. Retrieved from https://linkinghub.elsevier.com/retrieve/pii/S0022169411005701 doi: 10.1016/j.jhydrol.2011.08.024

Vandenbohede, A., Louwyck, A., & Lebbe, L. (2009, 1). Conservative solute versus heat transport in porous media during push-pull tests. *Transport in Porous Media*, *76*, 265-287. Retrieved from http://link.springer.com/10.1007/s11242-008-9246-4 doi: 10.1007/s11242-008-9246-4

Vanhoudt, D., Desmedt, J., Bael, J. V., Robeyn, N., & Hoes, H. (2011, 12). An aquifer thermal storage system in a belgian hospital: Long-term experimental evaluation of energy and cost savings. *Energy and Buildings*, *43*, 3657-3665. Retrieved from https://linkinghub.elsevier.com/retrieve/pii/S0378778811004427 doi: 10.1016/j.enbuild.2011.09.040

Villani, C. (2009). *Optimal Transport* (Vol. 338). Berlin, Heidelberg: Springer Berlin Heidelberg. Retrieved 2022-03-01, from http://link.springer.com/10.1007/978-3-540-71050-9 doi: 10.1007/978-3-540-71050-9

Vrugt, J. A. (2016, January). Markov chain monte carlo simulation using the DREAM software package: Theory, concepts, and matlab implementation. *Environmental Modelling & Software*, *75*, 273–316. Retrieved 2021-02-05, from https://linkinghub.elsevier.com/retrieve/pii/S1364815215300396 doi: 10.1016/j.envsoft.2015.08.013

Vrugt, J. A., & Robinson, B. A. (2007, 1). Treatment of uncertainty using ensemble methods: Comparison of sequential data assimilation and bayesian model averaging. *Water Resources Research*, *43*. Retrieved from http://doi.wiley.com/10.1029/2005WR004838 doi: 10.1029/2005WR004838

Wagner, V., Li, T., Bayer, P., Leven, C., Dietrich, P., & Blum, P. (2014, 2). Thermal tracer testing in a sedimentary aquifer: field experiment (lauswiesen, germany) and numerical simulation. *Hydrogeology Journal*, *22*, 175-187. Retrieved from http://link.springer.com/10.1007/s10040-013-1059-z doi: 10.1007/s10040-013-1059-z

Wildemeersch, S., Jamin, P., Orban, P., Hermans, T., Klepikova, M., Nguyen, F., ... Dassargues, A. (2014, 11). Coupling heat and chemical tracer experiments for estimating heat transfer parameters in shallow alluvial aquifers. *Journal of Contaminant Hydrology*, *169*, 90-99. Retrieved from https://linkinghub.elsevier.com/retrieve/pii/S0169772214001247 doi: 10.1016/j.jconhyd.2014.08.001

Wöhling, T., & Vrugt, J. A. (2008, 12). Combining multiobjective optimization and bayesian model averaging to calibrate forecast ensembles of soil hydraulic models. *Water Resources Research*, *44*. Retrieved from http://doi.wiley.com/10.1029/2008WR007154 doi: 10.1029/2008WR007154

Yin, Z., Strebelle, S., & Caers, J. (2020, 2). Automated monte carlo-based quantification and updating of geological uncertainty with borehole data (autobel v1.0). *Geoscientific Model Development*, *13*, 651-672. Retrieved from https://gmd.copernicus.org/articles/13/651/2020/ doi: 10.5194/gmd-13-651-2020

Zhang, J., Zeng, L., Chen, C., Chen, D., & Wu, L. (2015, 1). Efficient bayesian experimental design for contaminant source identification. *Water Resources Research*, *51*, 576-598. Retrieved from http://doi.wiley.com/10.1002/2014WR015740 doi: 10.1002/2014WR015740

Zhang, J., Zheng, Q., Chen, D., Wu, L., & Zeng, L. (2020, 1). Surrogate-based bayesian inverse modeling of the hydrological system: An adaptive approach considering surrogate approximation error. *Water Resources Research*,

56. Retrieved from https://onlinelibrary.wiley.com/doi/10.1029/2019WR025721 doi: 10.1029/2019WR025721

Zhou, H., Gómez-Hernández, J. J., & Li, L. (2014, January). Inverse methods in hydrogeology: Evolution and recent trends. *Advances in Water Resources*, *63*, 22–37. Retrieved 2021-01-20, from https://linkinghub.elsevier.com/retrieve/pii/S0309170813002017 doi: 10.1016/j.advwatres.2013.10.014